

THE IRON LINE BACKGROUND

MARCELLA BRUSA

Max Planck Institut für extraterrestrische Physik, Giessenbachstrasse 1, D-85748 Garching, Germany

ROBERTO GILLI

INAF – Osservatorio Astrofisico di Arcetri, Largo E. Fermi 5, I-50125 Firenze, Italy

ANDREA COMASTRI

INAF – Osservatorio Astronomico di Bologna, via Ranzani 1, I-40127 Bologna, Italy

Draft version December 3, 2018

ABSTRACT

We investigate the presence of iron line emission among faint X-ray sources identified in the 1Ms *Chandra* Deep Field South and in the 2Ms *Chandra* Deep Field North. Individual source spectra are stacked in seven redshift bins over the range $z = 0.5-4$. We find that iron line emission is an ubiquitous property of X-ray sources up to $z \simeq 3$. The measured line strengths are in good agreement with those expected by simple pre-*Chandra* estimates based on X-ray background synthesis models. The average rest frame equivalent width of the iron line does not show significant changes with redshift.

Subject headings: Surveys – Galaxies: active — X-rays: galaxies – X-rays: general – X-rays: diffuse background

1. INTRODUCTION

It has been pointed out already a decade ago (Matt & Fabian 1994) that prominent spectral features, and especially the ~ 6.4 keV iron $K\alpha$ emission line commonly found in Seyferts spectra (Nandra & Pounds 1994), may lead AGN synthesis models to predict a detectable signature in the spectrum of the cosmic X-ray background (XRB) around a few keV.

The integrated contribution of iron line emission in the sources making the XRB has been quantitatively estimated by Gilli et al. (1999), on the basis of a large database of observational results available in the pre-*Chandra* and XMM-*Newton* era. The predicted shape of the integrated emission from individual lines was computed following the prescriptions of the XRB synthesis model of Comastri et al. (1995) resulting in a rather broad bump extending from about 1 keV (depending on the maximum redshift assumed) up to 6.4 keV. The expected intensity of such a bump above the XRB level is below the 5% level over most of the energy range and reaches a maximum value of the order of 7% around 2–3 keV, the exact value being dependent on the redshift (z_{cut}) at which the evolution of the luminosity function is stopped. Although such an estimate is model dependent, Gilli et al. (1999) concluded that it can be safely regarded as an upper limit to the total iron line contribution.

In the last few years our knowledge of the XRB sources has been significantly improved by deep *Chandra* and XMM-*Newton* surveys. A fraction as large as 80–90% of the XRB flux below 5–6 keV has been resolved into individual sources (Worsley et al. 2004). Extensive multiwavelength follow-up observations have clearly established that the X-ray source redshift distribution is peaked at $z \simeq 0.7-1$ (e.g. Hasinger 2004, Gilli 2004) and that about 60% of the XRB originates at $z < 1$ (Barger et al. 2003). In the XRB synthesis model worked out

by Gandhi & Fabian (2003) the iron line contribution turned out to be maximum at about 3.8 keV (corresponding to a typical redshift of 0.7) and the excess due to the iron line is of the order of 3–4 %.

Despite the increasing number of independent observations of the XRB spectrum below 10 keV with BeppoSAX (Vecchi et al. 1999), XMM-*Newton* (De Luca & Molendi 2004) and RXTE (Revnivtsev et al. 2004), yielding good signal to noise ratio measurements of the extragalactic background, the accuracy reached so far is not such to detect the iron features at the level expected by the model predictions outlined above.

An alternative approach, devised to avoid the line smearing due to the large redshift range over which AGN spectra are summed and the present uncertainties in the XRB spectrum, is to search for iron features over appropriate redshift bins. The detection of an iron line and the study of its intensity and profile would open the possibility to investigate interesting issues such as the metal abundances and the relative fraction of Compton thick sources (which are known to have extremely strong iron lines) at high redshift, along with relativistically broadened lines beyond the local Universe (Comastri, Brusa, Civano 2004; Streblyanska et al. 2005). In the following we will present and discuss the results obtained for a large sample of spectroscopically identified sources in the X-ray surveys which resolved most of the XRB: the 2 Ms pointing in the *Chandra* Deep Field North (Alexander et al. 2003; hereinafter CDFN) and the 1 Ms observation of the *Chandra* Deep Field South (Giacconi et al. 2002; hereinafter CDFS). Throughout the paper, the adopted values for the Hubble constant and the cosmological parameters are $H_0=70 \text{ km s}^{-1} \text{ Mpc}^{-1}$, $\Omega_\Lambda=0.7$, $\Omega_m=0.3$.

2. DATA ANALYSIS

2.1. The sample

The optical spectroscopic and photometric redshifts of the X-ray sources detected in the CDFN are presented by Barger et al. (2003), while a list of spectroscopic redshifts of the sources detected in the CDFS is reported in Szokoly et al. (2004; hereinafter S04). Photometric redshifts based on good quality HST/ACS images and deep ISAAC/VLT observations are available for all but four CDFS sources without spectroscopic redshift (Zheng et al. 2004; hereinafter Z04), leading to a virtually complete catalog of identified X-ray sources. Here we have considered only those CDFS photo-z with a quality flag greater than 0.5 (see Z04 for details) ensuring a reliable redshift estimate. Moreover, given that both S04 and Z04 identifications are based on the X-ray source catalogue of Giacconi et al. (2002), we have revised some optical/X-ray associations according to the improved astrometry provided by Alexander et al. (2003). Only sources with spectroscopic redshifts have been included in the CDFN sample because no details are given on the photo-z quality in Barger et al. (2003). The larger CDFS redshift completeness allows us to obtain a counting statistic per redshift bin similar to that of the CDFN despite the shorter exposure.

Individual source spectra have been stacked together in seven redshift bins spanning the $z=0.5-4$ range (Table 1). The choice of bin sizes and distribution is driven by a trade-off between the number of counts in each bin and the need to sample a corresponding observed energy range narrow enough to detect the spectral feature, keeping at the same time the instrumental response as uniform as possible. For these reasons, the redshift interval below $z=0.5$ is not considered; moreover, the redshift interval $1.7 < z < 2.5$ is excluded because the iron line is redshifted in the $\sim 1.8-2.4$ keV energy range, which encompasses the sharp drop in the effective area due to the instrumental iridium edge.

The iron line signal is not expected to be significantly diluted by non-AGN sources. Below $z=2$, the $K\alpha$ line falls in the hard band (> 2 keV), where the detected sources are mostly AGN. At higher redshifts it is shifted to the soft band, but then only sources with AGN luminosities can be detected. In order to avoid contamination by a few individual bright sources which could dominate the stacked signal we have excluded from each bin the brightest object, if its contribution exceeds 50% of the entire flux in the bin. The chosen redshift bins, the expected position of the 6.4 keV line, the bin width and the number of sources in each bin are listed in Table 1. The final sample includes 171 sources in the CDFN and 181 in the CDFS, spanning the luminosity range $L_{2-10\text{keV}} = 10^{41} - 10^{45}$ erg s⁻¹ (see Table 1). The small solid angle (~ 0.2 deg⁻²) covered by the deep fields does not allow us to sample the AGN population at higher luminosities.

2.2. X-ray stacking

The X-ray data for both the CDFN and CDFS observations have been retrieved from the public archive and processed with standard tools making use of the calibrations associated with the CIAO¹ software (version 3.0).

A total of 20 and 11 pointings in the CDFN and CDFS, respectively, were summed together with the `merge_all`² script in two different merged event files. The Charge Transfer Inefficiency (CTI) and gain³ corrections were also applied to each single pointing⁴. Spectra, response matrices and effective areas of the stacked spectrum in each redshift bin were extracted from the merged event files using the standard CIAO tools developed to properly weight responses and effective area files for multiple extraction regions (e.g. `mkwarf`; see Civano, Comastri & Brusa 2005 for a detailed description of the procedure). The target positions in each redshift bin span almost all the off-axis angles, thus the extraction radius was varied from 4 to 16 arcsec depending on the source brightness and off-axis position. Several background spectra were extracted with the same procedure from a stack of regions nearby each source in each redshift bin and varied in size and shape.

Finally, the stacked spectra in each redshift bin of both the CDFN and CDFS were summed together with standard FTOOLS routines (`mathpha`, `addarf`, `addrmf`) weighted for both the exposure time and the number of counts. In the following we will consider only the resulting CDFN+CDFS spectra.

3. SPECTRAL ANALYSIS

Since we are interested in emission features over a well defined energy range, source spectra have been extracted in the 1–6 keV band, to minimize calibration uncertainties in the low energy response. X-ray spectra were rebinned to have at least 20 counts per bin and fitted with XSPEC (version 11.3.0; Arnaud 1996); errors are reported at the 90% confidence level for one interesting parameter ($\Delta\chi^2=2.71$).

The continuum is parameterized with a single power-law with the slope free to vary. A negative ($\tau = -0.17$) edge at 2.07 keV has been added to account for residual uncertainties in the effective area above 2 keV, as suggested by the CXC team (Vikhlinin et al. 2005)⁵. With the exception of the highest redshift bin, a significant excess above a power-law continuum is present over the energy range $6.4/(1+z_{max}) - 6.4/(1+z_{min})$ keV, where z_{min} and z_{max} are the bin boundaries (see Fig. 1). We then added a redshifted gaussian component (model `po+zgauss`) with the width free to vary, centroid energy fixed at 6.4 keV and redshift fixed at the mean value of each bin (\bar{z}), and verified that in all cases the fit improved, though with a different level of significance. Table 1 lists the best fit parameters for each redshift bin. The equivalent widths (EWs) quoted in Table 1 are measured

¹ <http://cxc.harvard.edu/ciao/>

² http://cxc.harvard.edu/ciao3.0/threads/merge_all/

³ <http://hea-www.harvard.edu/alexey/acis/tgain>

⁴ We have also verified that applying the new gain correction tool released with the CALDB 2.28 version the results are not modified.

⁵ See also: http://cxc.harvard.edu/ccw/proceedings/03_proc/presentations/marshall2

in the observed frame. To get the intrinsic, rest frame EWs a multiplicative factor $1 + \bar{z}$ must be applied⁶.

3.1. Safety checks

In order to check whether the results are dependent from the counting statistics and/or the energy range over which the continuum underlying the iron excess is measured, we have performed several safety checks.

First, we have further excluded in each bin the two or three brightest sources, if their contribution to the total counts was larger than 60%. Then, spectral fits were repeated in the 2.2–6 keV energy range for sources at $z < 2$. Finally, a redshifted absorption component (assumed to be at \bar{z} in each redshift bin) was added to the continuum. In all cases, the spectral parameters were found in agreement, within the statistical errors, with those reported in Table 1. Furthermore, for the $z < 2$ bins for which the statistics is higher, we verified that, when the redshift of the line component is left free to vary, the resulting best fit redshift is always almost coincident with that expected from a line at 6.4 keV.

Extensive simulations have also been performed to quantitatively assess the line broadening introduced by redshift smearing. The spectra of the sources contributing to each bin were modeled as a single power law plus a narrow unresolved ($\sigma=0.1$ keV) $K\alpha$ line. The actually observed sources redshift distribution within the bin is further assumed and the individual simulated spectra are stacked together. With the exception of the $z=0.9-1.1$ bin, all the measured widths are in agreement with those resulting from the simulations, and therefore consistent with being produced by the superposition of narrow features (but see also the discussion).

According to XRB synthesis models, a large fraction of the sources contributing to each redshift bin are obscured by column densities in the range $\sim 10^{22-24}$ cm^{-2} . When obscured sources at different redshifts are stacked together, the iron line underlying continuum is expected to be modified, with respect to a single power law, by the most prominent absorption features such as the low energy cut-off and the 7.1 keV iron edge. To take this into account, we assumed a continuum shape as resulting from the Gilli et al. (2001) model once the AGN luminosity function is integrated in the narrow redshift bins adopted here. Although the recomputed EW are lower than those reported in Table 1 (by about 30-50%), the line excess is still significant. A more detailed investigation would require an extensive analysis of the AGN synthesis models parameter space and is beyond the purposes of this letter.

⁶ The superposition of sources at different redshift in each bin should return a slightly different multiplicative factor, but the difference in the rest frame EW obtained by using $(1 + \bar{z})$ is negligible.

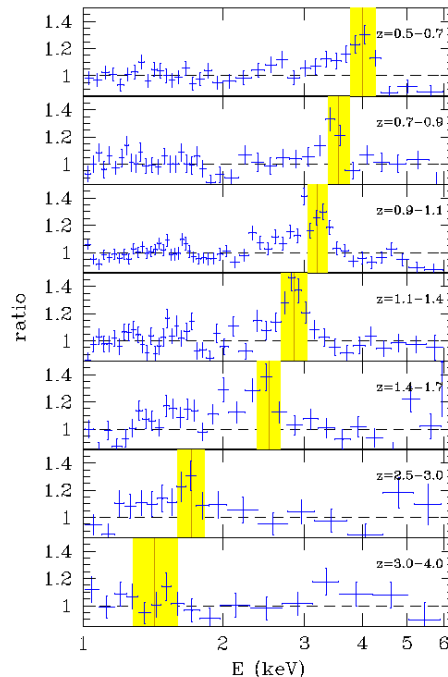


FIG. 1.— Residuals of a simple power-law fit to the source spectra in seven different redshift bins as labeled. The vertical line in each panel is at the expected position for the redshifted 6.4 keV Fe $K\alpha$ line while the shaded region encompasses the bin width reported in Table 1 and defined as $\Delta E = 6.4/(1+z_{max}) - 6.4/(1+z_{min})$ keV.

4. DISCUSSION

The rest frame equivalent widths for the seven redshift bins are compared (Fig. 2) with those predicted by the XRB synthesis model of Gilli et al. (2001, shaded area in Fig. 2). The line EW distribution is modeled following Gilli et al. (1999, see their Table 4) and is a function of the absorption column density increasing from about 250 eV for unobscured sources, to 400 eV for obscured ($\log N_H < 24$) AGN, reaching about 2 keV for Compton thick sources. These values are constant over the entire redshift range. The upper bound of the shaded region has been computed assuming $\text{EW}=280$ eV for unobscured sources, consistent with the average value measured by ASCA in the nearby Universe. Recent XMM-*Newton* and *Chandra* results have questioned the presence of broad iron lines in many unobscured-type 1 AGN, measuring in turn a lower EW ($\sim 100-150$ eV on average) along with a decrease of the line EW towards high luminosities (e.g. Page et al. 2004). We have quantitatively estimated the effects of reducing the line EW among unobscured sources by considering the most conservative case of no iron emission at all (lower bound in Fig. 2). Since in our model most of the iron signal is produced by obscured sources with $22 < \log(N_{mH}) < 24$ cm^{-2} , the overall EW are reduced by only 15–20%.

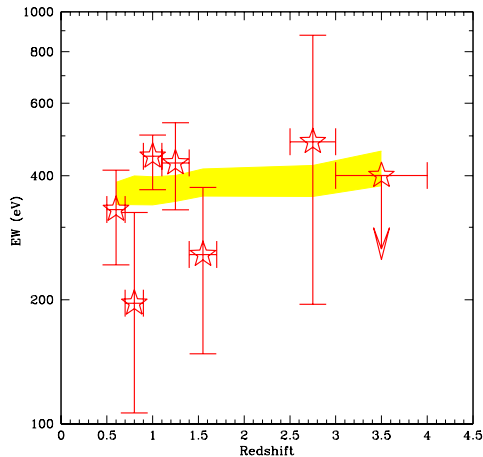


FIG. 2.— Rest frame equivalent widths as a function of redshift compared with the model predictions (shaded strip; see text for details).

The lack of any dependence of the average line intensity upon redshift up to $z \sim 3$ could be naively interpreted as a constant iron abundance with redshift. The real case is likely to be much more complicated, given the several factors affecting the detected signal. As an example, the population of heavily obscured Compton thick sources (which have the strongest iron lines) might be hiding among the X-ray sources either unidentified or with a poorly constrained photo- z and thus not included in the present analysis. However, according to our calculations (Gilli et al. 2001), Compton Thick AGN are expected to provide only about 5–10% of the iron signal in each redshift bin. The presence of a population of Compton Thick sources much larger than that assumed would be more easily appreciated by the distortions introduced on the broad band 3–100 keV XRB spectrum rather than by a stronger line in the various redshift bins.

A significant decrease of the line EW towards high luminosities has been reported by Nandra et al. (1997) for a sample of type 1 AGN observed with ASCA. The effect is more pronounced for luminosities higher than 10^{45} erg s^{-1} . Unfortunately, our sample is not well suited to investigate iron line properties at high luminosities due to the lack of sources luminous enough (see Table 1) to check the Nandra et al. (1997) findings. Moreover, the stacked spectra are dominated by obscured sources rather than type 1 AGN adding further uncertainties in the comparison.

Our findings are also consistent with those reported by Streblyanska et al. (2005) from the analysis of the rest-frame stacked spectrum of identified sources in the XMM-Newton observation of the Lockman Hole (~ 400 eV, when a gaussian profile is considered). The residuals leftward of the iron line which in our fits are more prominent in the bins with the highest number of sources and counting statistic ($z=0.5-0.7$ and $0.9-1.1$) suggest the presence of a broad redshifted component, similar to that observed by Streblyanska et al. (2005). Since the main goal of the present analysis is the detection of iron emission in the sources of the XRB up to high redshifts, our approach is not designed to investigate in detail the average line shape. We recall, however, that the observed EW and line profile are dependent on an accurate modeling of the underlying continuum. The superposition of absorbed spectra with different redshifts has the effect of reducing the measured EW (see previous Section) and furthermore may produce a spurious red wing.

5. SUMMARY

We report the detection of iron emission up to $z \sim 3$ in the X-ray spectra of faint *Chandra* sources stacked into different redshift bins. The measured EW are in agreement with a scenario in which the lines are intrinsically narrow and their intensity does not change significantly with redshift (and/or luminosity), which can be interpreted as a constant iron abundance as a function of redshift. Extensive simulations and safety checks have been performed in order to test the reliability of our results. Even taking into account the effects of absorption features which modify the high energy power law in obscured sources the detection of the emission line remains significant. Despite their prominent iron lines, our approach does not allow to put tight constraints on the number density of Compton Thick sources, that suffer from extreme absorption in the *Chandra* band and can be detected only in small numbers compared to Compton thin AGN. Although there might be hints for the presence of gravitationally redshifted broad line components, we caution that their intensity and profile significantly depends on the modeling of the underlying continuum.

We gratefully thank Francesca Civano and Piero Ranalli for help in data reduction, Giorgio Matt, Gianni Zamorani, Cristian Vignali, Paolo Tozzi and Giancarlo Setti for useful discussions. We acknowledge partial support from MIUR Cofin-03-02-23 and INAF/270/2003 grants.

REFERENCES

- Alexander, D.M., Bauer, F.E., Brandt, W.N., et al. 2003, *AJ*, 126, 539
 Barger, A., Cowie, L., Capak, P., et al. 2003, *AJ*, 126, 632
 Civano, F., Comastri, A., & Brusa, M. 2005, *MNRAS*, in press, [astro-ph/0501397]
 Comastri, A., Setti, G., Zamorani, G., Hasinger, G., 1995, *A&A*, 296, 1
 Comastri, A., Brusa, M., Civano, F. 2004, *MNRAS*, 351, L9
 De Luca, A., & Molendi, S. 2004, *A&A*, 419, 837
 Gandhi, P., & Fabian, A.C. 2003, *MNRAS*, 339, 1095
 Giacconi, R., et al. 2002, *ApJS*, 139, 369
 Gilli, R., Comastri, A., Setti, G. & Brunetti, G., 1999, *New Astronomy* 4, 45
 Gilli, R., Salvati, M., & Hasinger, G. 2001, *A&A*, 366, 407
 Gilli, R. 2004, *Adv. Sp. Res.*, 34, 2470
 Hasinger G. 2004, in “BeppoSAX 2003”, *Nucl. Physics B (Proc. Suppl.)*, 132, 86
 Matt, G., Fabian, A.C., 1994, *MNRAS*, 267, 187
 Nandra, K., Pounds, K.A., 1994, *MNRAS*, 268, 405
 Nandra, K., George, I.M., Mushotzky, R.F., Turner, T.J., Yaqoob, T., 1997, *ApJ*, 488, L91
 Page, K.L., O’Brien, P.T., Reeves, J.N., and Turner, M.J.L., 2004, *MNRAS*, 347, 316
 Revnivtsev, M., Gilfanov, M., Sunyaev, R., Jahoda, K., & Markwardt, C. 2004, *A&A*, 411, 329
 Streblyanska, A., Hasinger, G., Finoguenov, A., Barcons, X., Mateos, S., & Fabian, A.C. 2005, *A&A* in press, [astro-ph/0411340]

Szokoly, G.P., Bergeron, J., Hasinger, G., et al 2004, ApJS, 155, 271
 Vikhlinin, A., Markevitch, M., Murray, S.S., Jones, C., Forman, W., & Van
 Speybroeck, L. 2005, ApJ in press, astro-ph/0412306
 Vecchi, A., Molendi, S., Guainazzi, M., Fiore, F., & Parmar, A.N. 1999, A&A,
 349, L73

Worsley, M.A., Fabian, A.C., Barcons, X., Mateos, S., Hasinger, G., & Brunner,
 H. 2004, MNRAS, 352, L28
 Zheng, W., Mikles, V.J., Mainieri, V., et al. 2004, ApJS, 155, 73

TABLE 1
 REDSHIFT BINS AND NUMBER OF SOURCES

$z^{(1)}$	$E(K\alpha)^{(2)}$	Bin width ⁽³⁾	Number of sources ⁽⁴⁾			$\langle L_X \rangle^{(5)}$	Counts ⁽⁶⁾	$\Gamma^{(7)}$	PL + zgauss ⁽⁸⁾	$\Delta\chi^2$ ⁽⁹⁾	$\sigma^{(10)}$	EW ⁽¹¹⁾
min-max	keV	keV	CDFS	CFDN	Total	$10^{42} \text{ erg s}^{-1}$		$\chi^2/\text{d.o.f.}$			keV	eV
0.5-0.7	4.00	0.50	45(7)	39	84	1(0.1-140)	16831	1.20±0.03	284.2/289	44.2	0.30 $^{+0.12}_{-0.09}$	207 $^{+31}_{-55}$
0.7-0.9	3.55	0.40	34(10)	32	66	4(0.3-300)	13240	1.44±0.04	229.7/260	14.0	0.27 $^{+0.78}_{-0.14}$	116 $^{+68}_{-58}$
0.9-1.1	3.20	0.32	30(11)	58	88	8(0.6-400)	34958	1.47±0.02	342.6/321	112.6	0.48 $^{+0.14}_{-0.12}$	223 $^{+28}_{-36}$
1.1-1.4	2.78	0.38	25(10)	25	50	20(0.9-400)	15629	1.45±0.04	258.3/267	63.8	0.31 $^{+0.15}_{-0.12}$	191 $^{+48}_{-44}$
1.4-1.7	2.56	0.30	19(11)	4	23	40(2-500)	7841	1.36±0.04	248.0/195	19.0	0.18 $^{+0.18}_{-0.18}$	101 $^{+46}_{-43}$
2.5-3.0	1.71	0.23	18(9)	4	22	100(20-1000)	4895	1.46±0.07	164.5/141	10.0	1.15 $^{+0.61}_{-0.40}$	129 $^{+105}_{-77}$
3.0-4.0	1.42	0.32	9(3)	9	18	200(36-2000)	2919	1.30±0.10	82.3/111	2.0	< 1.94	< 89

Notes: ⁽¹⁾Redshift range for the stacked spectra. ⁽²⁾Expected position of the Fe 6.4 keV line in the observed frame. ⁽³⁾Observed frame bin width, in keV, at the 6.4 keV position. ⁽⁴⁾Number of sources in the CDFS, CFDN and combined samples (in parenthesis for the CDFS sources with photometric redshifts). ⁽⁵⁾Median 2-10 keV luminosity (in parenthesis the minimum and maximum luminosities) ⁽⁶⁾Total net counts in the 1-6 keV band. ⁽⁷⁾Best fit power-law spectral index and 90% errors. ⁽⁸⁾Statistical significance of the spectral fit for the p+ zgauss model. ⁽⁹⁾ $\Delta\chi^2$ with respect to the single power-law model. ^(10,11)Best fit line width (σ) and observed frame intensity (EW) of the gaussian component and 90% errors.